Solid Freeform Fabrication 2024: Proceedings of the 35th Annual International Solid Freeform Fabrication Symposium – An Additive Manufacturing Conference
Reviewed Paper

INFLUENCE OF LAYER PITCH EXPANSION FOR PBF-LB/P EFFICIENCY IMPROVEMENT ON PART STRENGTH

Yuki Yamauchi[1], Koichi Fujii[1], Takashi Kigure[1,2], Toshiki Niino[2], Hirofumi Nonaka[3], and Mitsuhiro Kumasaka[3]

1 Tokyo Metropolitan Industrial Technology Research Institute, 2-4-10 Aomi Koto-ku, Tokyo, Japan
2 Institute of Industrial Science, the University of Tokyo, 4-6-1 Komaba Meguro-ku, Tokyo, Japan
3 ASPECT Inc., 6-17-10 Nagayama Tama-shi, Tokyo, Japan

Abstract

Although PBF-LB/P is one of the most promising additive manufacturing technologies for part production, the industries that use it are limited. One reason for this limitation is the production cost of PBF-LB/P, which can be reduced by increasing process efficiency, such as production speed. In this study, to improve the production speed of PBF-LB/P, we attempted to expand the layer pitch, which is called the layer thickness, that is, the distance of platform movement per layer. The layer pitch can affect the interlayer adhesion or part strength. Herein, the relationship between layer pitch and tensile strength in the z-direction was investigated. Because the energy required to melt the supplied powder per layer also varies with the layer pitch, process parameters such as the energy density of laser exposure per layer were adjusted when the specimens were built.

Introduction

Powder Bed Fusion for polymeric materials with a laser beam (PBF-LB/P) does not necessitate the design and construction of a structure to support the processed region. This enables efficient utilization of a build envelope and higher productivity than other additive manufacturing processes[1]. However, in comparison to other manufacturing processes such as injection molding, the productivity of PBF-LB/P is still extremely low. Depending on the shape or size of the part, the production cost of PBF-LB/P is higher than that of injection molding, even including the initial cost of mold preparation, when the number of parts exceeds hundreds[2]. This limits the utilization of PBF-LB/P in the production of end-use parts, such as small-scale production or production in specific industries that prioritize part complexity or reduce labor costs in assembly. Therefore, lowering the production cost of PBF-LB/P could enable a large number of applications for which injection molding could be replaced. To reduce production costs, it is not sufficient to reduce the cost of PBF machines and materials; improving productivity is also necessary. For example, higher process speeds reduce the operating time per batch and machine and system depreciation. In recent years, several attempts have been made to reduce the processing time per layer using infrared lamps and inkjet processes. These attempts have led to the commercialization of various processes, including High Speed Sintering, Multi Jet Fusion, Selective Absorption Fusion®, and others.

In the context of metal powder bed fusion processes (PBF-LB/M), some research groups have attempted to set a larger layer pitch (here, the layer pitch means a displacement of the build platform per layer, which is well known as “layer thickness”; both are clearly distinguished in this paper because the layer thickness can vary depending on an apparent a density of powder and processed region[3]) to reduce the number of layers per batch for high-speed processing[4]. Simply, the processing time will be approximately twice as fast when the layer pitch is doubled for the same layer time. Numerous layer pitch settings have already been employed to accommodate various materials, powder sizes, and other factors in commercially available PBF-LB/M.

By contrast, the pitch of PBF-LB/P is typically set at 100 μm in the majority of commercial systems and is not varied significantly. Some authors have tested layer pitches of 80–150 μm and investigated the influence of layer pitch expansion on built part quality[5][6][7][8]. However, the change in pitch was relatively minor compared to the typical pitch. Although a report exists in which specimens were prepared in a 200 μm pitch, it did not mention building parameters such as input energy optimization[9]. Consequently, large-layer pitches have not yet been investigated in detail. As indicated in reports addressing the issue of layer pitch expansion, there was a notable increase in the anisotropy of the mechanical properties of the built part. This is attributed to the reduction in the strength of the part in the direction of the layer. One of the reasons for the reduction in the part strength in the layer direction is the lower adhesion between the layers, specifically the connection between the n^{th} and $n\text{-}1^{th}$ layers. To facilitate the connection between the layers, the n^{th} layer is subjected to laser exposure, resulting in a molten region that extends to the previously processed $n\text{-}1^{th}$ layer. It is relatively straightforward to envisage that the connection becomes more challenging as the layer pitch increases. This connection can be reinforced by applying high energy[10] to increase the melting depth, which is the depth of fusion[11]. Moreover, a strong correlation exists between the depth of fusion and the depth at which the incident light penetrates the powder layer, referred to as the penetration depth [12]. Thus, expanding the penetration depth is also effective in enhancing the connection [13]. However, because the CO_2 laser, which is most commonly used in conjunction with commercially available PBF-LB/P, is highly absorbed by most polymer materials, the penetration depth is equal to or less than the typical layer pitch[14]. Consequently, the temperature near the surface increased to a much higher level, and the thermal degradation of materials near the surface due to thermal decomposition or sublimation is a concern. Therefore, to apply layer pitch extension to PBF-LB/P for CO_2 lasers, it is necessary to conduct investigations to ascertain the extent to which the pitch can be set without thermal degradation of the powder near the surface and the degree of strength that can be achieved simultaneously.

In this study, specimens with varying layer pitch and input energy were prepared, and their mechanical properties were tested. Additionally, the condition of the melting region or thermal degradation occurring at each input energy was estimated by various methods, including measuring the part density and observing the powder bed during laser irradiation, which are closely related to thermal degradation. The microstructures of the fabricated specimens were then evaluated. The results of the aforementioned experiment are discussed in this paper, with a particular focus on the relationship between the input energy and maximum part strength in each layer pitch, taking into account thermal degradation.

Material and Methods

Specimen preparation

Two specimen types were prepared: a block-shaped specimen was designed for density measurement and microstructure observation, whereas a dog bone-shaped specimen defined in ISO 3167:2002 was intended for tensile testing. Their dimensions were 20 mm ×10 mm ×5 mm and 80 mm ×10 mm ×2 mm (which is half the size of the standard, and the parallel section was 30 mm). The block-shaped specimens were oriented as 5 mm ×20 mm ×10 mm. For the dog bone-shaped specimens, the longitudinal side (80 mm) was oriented along the z-axis, which was the layering direction.

The specimens were prepared using PA11 powder (ASPECT Inc., ASPEX-FPA) and a PBF-LB/P machine (ASPECT Inc., RaFaEl 300C). The powder material was premixed in a 30:70 ratio, with 30% component representing the virgin material and 70% component representing the recycled material, which was then sieved. The PBF-LB/P machine was equipped with a CO_2 laser (with a maximum output of 60 W) and its beam diameter at the powder bed was 320 μm. Given that the processing region was between the melting point and the recrystallization point[15], the powder bed temperature was set at 185 °C. The layer pitch was selected as 100, 200, and 300 μm. As previously stated, an increase in the layer pitch results in an increased amount of powder or a thicker powder layer in each layering process. To adequately melt the powder, the input energy must be adjusted to accommodate the selected layer pitch. Furthermore, to enable a valid comparison of part strength across different pitch settings, it is essential to ensure that the input energy is consistent. This can be achieved by employing the appropriate theoretical models or indices. In this study, an Energy Melt Ratio (EMR, see Equation 1[16]) proposed in previous research was employed as an index of input energy, with a range of 4.0–8.0 set for all specimens and pitches, in accordance with Vasques's report[17].

$$EMR = \frac{\frac{P}{SS \times v}}{\left[C_p(T_m - T_b) + h_f\right] \times \rho_p \times l_z}, \tag{1}$$

where, P, SS, v, C_p, T_m, T_b, h_f, ρ_p, l_z are laser power, scan spacing, scan speed, specific heat, melting point, powder bed temperature, heat of fusion, apparent density of powder, and layer pitch, respectively.

The parameters listed in Table 1 were quoted from the specification sheet for the same type of material provided by other manufacturers[18]. The apparent density of the premixed powder, measured in advance by the authors, was 0.40 g/cm³. Table 2 lists the exposure parameters of each layer pitch. Contour scanning was not performed to avoid complex discussions.

Table 1 Specifications of PA11 powder

Melting point °C	201
Specific heat J/g K	2.09
Heat of fusion J/g	83.7
True density g/cm^3	1.04

Table 2 Exposure parameters for each layer pitch

Layer pitch μm	100	200	300
Laser power W	6–10	12–18	17–27
Scan speed m/s	2.0		
Scan spacing μm	130		

Tensile Test

Tensile tests were conducted using a universal testing system (INSTRON, 3366) and extensometer (INSTRON, 2630-120) to determine the mechanical properties of the prepared specimens. The ultimate strength (UTS), Young's modulus, and elongation at break (EaB) were obtained using an analysis software (INSTRON, Bluehill). The test speed in the strain range of 0.05%–0.25% was 0.5 mm/min, and the other range was fixed at 5.0 mm/min.

Relative Density

As the powder particles melt and the molten plastic flows, the gap between them is filled and the built parts become dense. The relative density, which is the ratio of the part density to the true density, is a convenient index for determining the conditions of the melt region. The part density was measured based on the Archimedes method using a hydrometer (SHIMADZU Corp., AUX220).

Microstructure observation

The microstructure of the built specimen provided insights into the conditions of the melting region and the connections between the layers. A thin specimen was cut from the center of the built part using a microtome (YAMATO KOKI INDUSTRIAL, RX-860) and observed using a transmission microscope with polarized light (KEYENCE, VHX-5000).

Results and Discussion

Mechanical Properties

Figures 1, 2, and 3 illustrate the results for the UTS, Young’s modulus, and elongation at break, respectively. Overall, there was a positive correlation between the EMR and the mechanical properties. At the same level of EMR, each mechanical property decreased as the layer pitch increased. Additionally, the maximum value of each mechanical property obtained in this study decreased as the layer pitch increased. For a layer pitch of 200 μm, the maximum value of UTS and Young’s modulus is reached at EMR 7, and they remain in a plateau or decline in EMR >7. For a layer pitch of 300 μm, no results were obtained in EMR <6, as the dog bone specimens were too weak to handle or test, particularly since delamination occurred before the test. These findings suggest that the interlayer connections become increasingly challenging as the layer pitch increases.

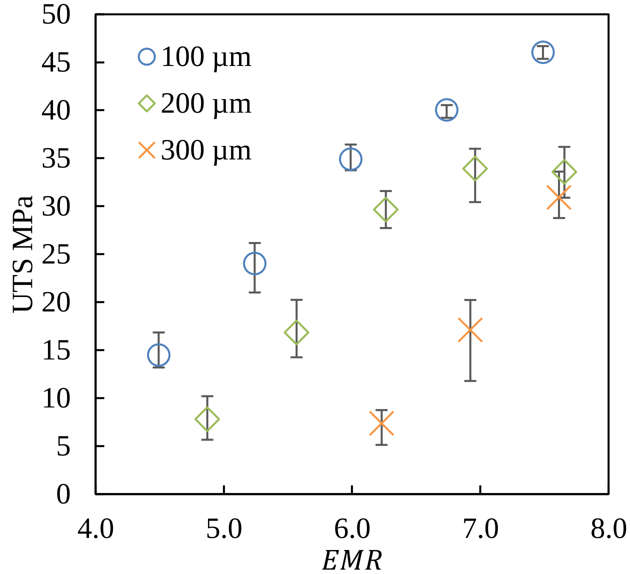

Figure 1 UTS for each layer pitch prepared under EMR 4.0–8.0. The plots of circles, diamonds, and crosses represent a layer pitch of 100, 200, and 300 μm, respectively. The error bars indicate the maximum and minimum values obtained from five samples in each condition.

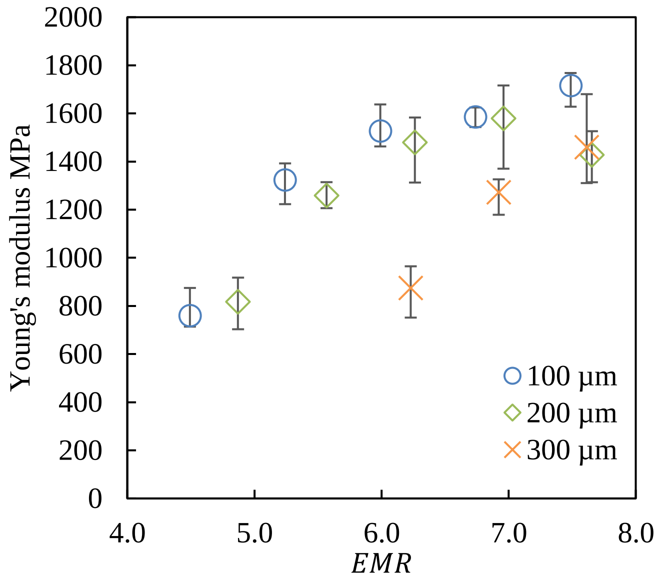

Figure 2 Young's modulus for each layer pitch under EMR 4.0–8.0. The types of plots and the number of samples are consistent with those depicted in Figure 1. The error bars indicate the maximum and minimum values obtained from five samples in each condition.

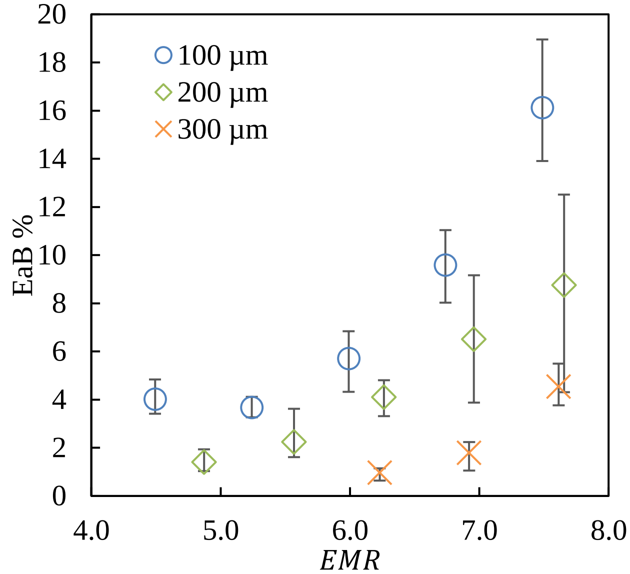

Figure 3 Elongation at break for each layer pitch under EMR 4.0–8.0. The types of plots and the number of samples are consistent with those depicted in Figure 1 and 2. The error bars indicate the maximum and minimum values obtained from five samples in each condition.

Relative Density

Figure 4 shows the relationship between the relative densities of the block-shaped specimens and EMR. The relative density for a layer pitch of 100 µm pitch increases with increasing EMR, in a manner analogous to the tendency of the mechanical properties. By contrast, the densities for 200 and 300 µm pitch reach their maximum value around EMR 5.5. Decreasing the densities in EMR >5.5 may be attributed to thermal decomposition. Nevertheless, even when the pitch is extended to 300 µm, it is still possible to obtain relatively dense parts, as evidenced by the block-shaped specimens presented here. This indicates that the powder material melted well.

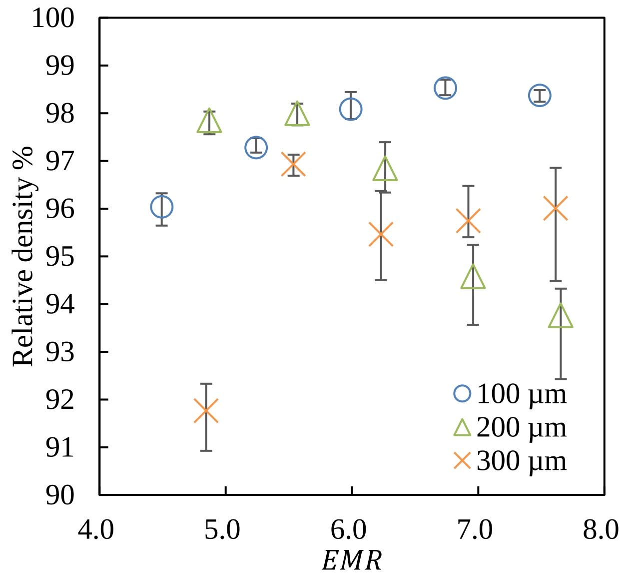

Figure 4 Relationship between EMR and relative density. The types of plots and the number of samples are consistent with those depicted in Figure 1–3. The error bars indicate the maximum and minimum values obtained from five samples in each condition.

Microstructure Observation

Figure 5 presents the cross-sectional images obtained using transmitted light microscopy for each condition. In all the images with EMR <6, the horizontally long voids near the interlayer are reduced, and the spherical voids increase as the EMR increases. For layer pitches of 100 and 300 µm, the same trends are observed in EMR >6. By contrast, horizontally long voids reappeared in EMR >7. To facilitate comparison of both microstructures, the transmission image with polarized light for a layer pitch of 200 µm, EMR of 4.9 and 7.7 in which the horizontally long voids were observed, is shown in Figure 6. In the microstructure of the low EMR, stripes appear at a periodicity of 200 µm. According to a previous study by Zarringhalam et al.[19], a low-degree melting region remains particularly near the interlayer at low input energy. Therefore, the stripe formation observed in this study can be attributed to insufficient melting. By contrast, the microstructure of the high EMR has no stripe pattern and appears to be relatively uniform, except the voids. This observation suggests that the powder material was sufficiently melted during the process under high EMR conditions and that the formation mechanism of the horizontally long void differed from that of the low EMR process. The voids are larger than those in the low EMR process, and spherical voids coexist. However, further investigation is necessary to gain a more comprehensive understanding.

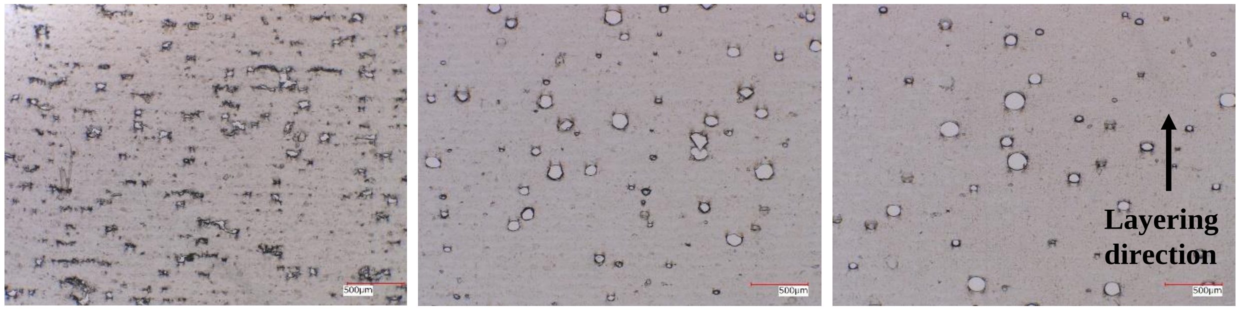

EMR 4.5 EMR 6.0 EMR 7.6

a) 100 µm

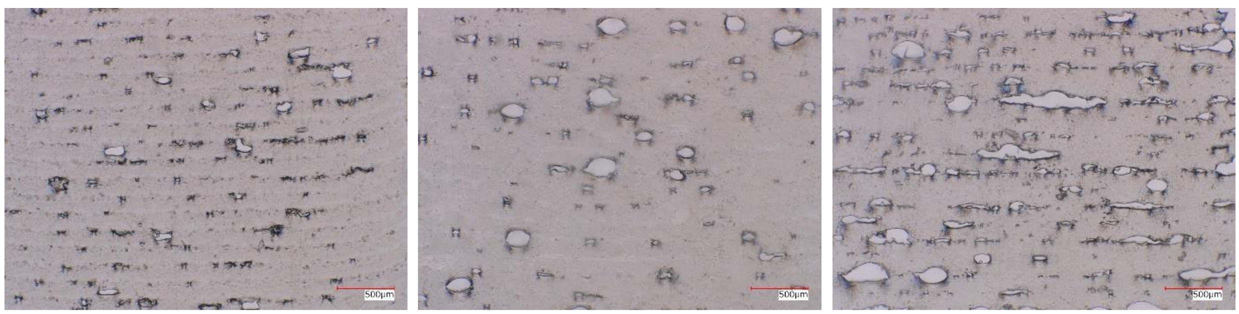

EMR 4.9 EMR 6.3 EMR 7.7

b) 200 µm

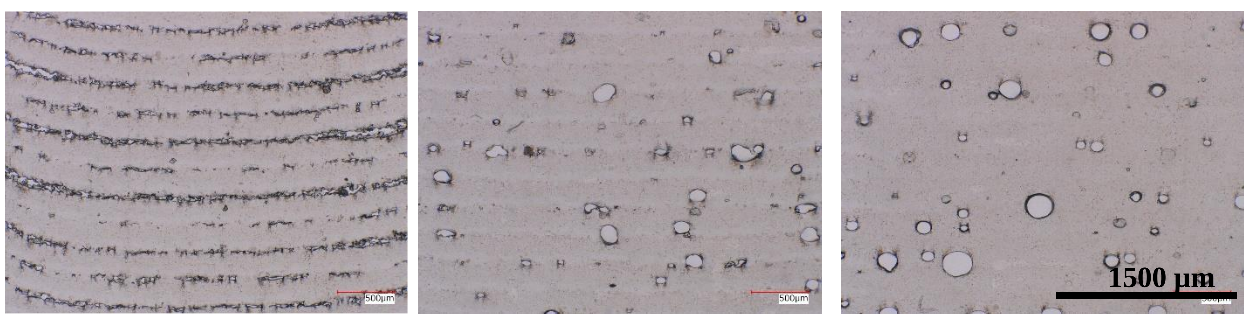

EMR 4.8 EMR 6.2 EMR 7.6

c) 300 µm

Figure 5 Cross-sectional image of specimens

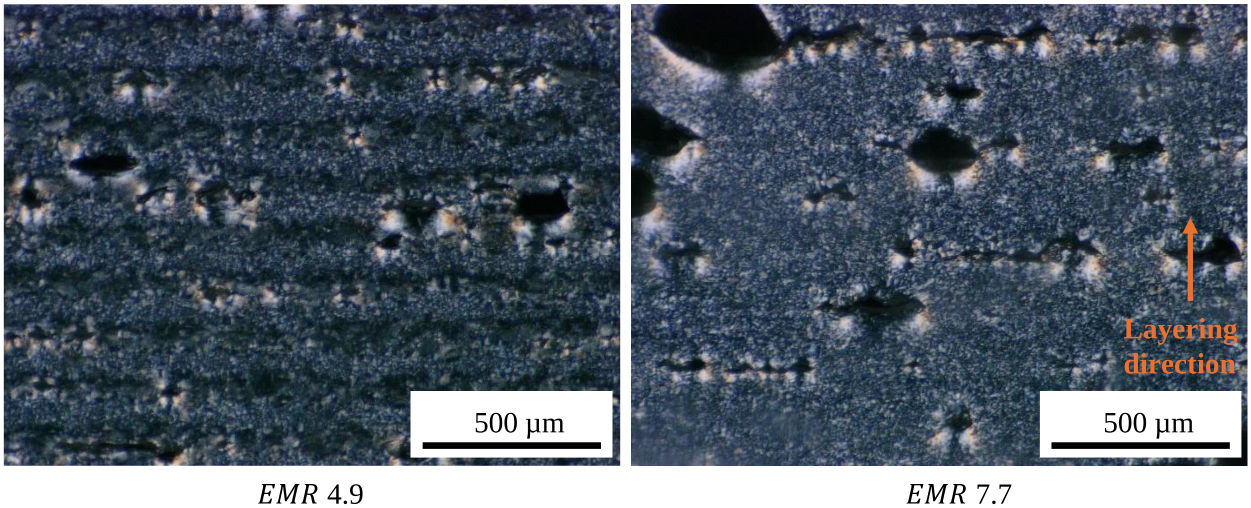

Figure 6 Cross-sectional view of 200 μm pitch using polarized transmission microscopy. The layering direction is from bottom to top.

<u>Observation during laser irradiation</u>

The powder bed was meticulously observed through an observation window during the laser irradiation to ascertain the generation of smoke and sparks associated with thermal degradation[20][21], which is a concern when high energy is supplied. Sparks were not observed under most conditions. As long as it was observed by the naked eye, smoke was also not observed under all conditions for a layer pitch of 100 μm. By contrast, smoke was observed in EMR >6 for a layer pitch of 200 μm and in all conditions for a layer pitch of 300 μm. Furthermore, smoke generation increased significantly with increasing input energy and layer pitch, even at the same EMR. As stated in the Materials and Methods section, even if the EMR was set to the same value, the actual input energy was greater when the layer pitch was larger. Therefore, smoke generation is simply a consequence of a high-energy input.

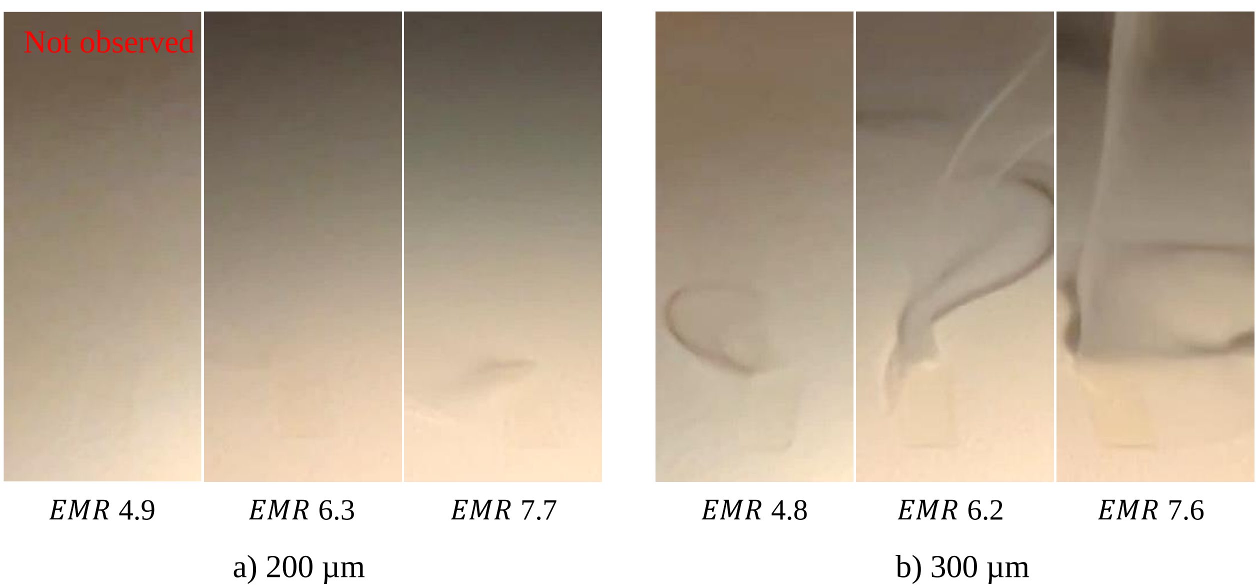

Figure 7 Captured images of powder bed during laser irradiation

Relationship between mechanical properties and processing condition for each pitch

Firstly, for a layer pitch of 100 μm, the mechanical properties may not have reached the maximum value yet. Specifically, a higher value was obtained for EMR > 7.6. However, there is still a slight room for improvement of the mechanical properties because they have already been achieved relatively close to the value reported in previous reports and data sheets provided by machine or powder manufacturers [15].

Secondly, in the case of a layer pitch of 200 μm, the UTS and Young's modulus reach the maximum value at EMR 7.0, but smoke is already generated at the energy of EMR>6. Assuming that the smoke generation and density decrease observed in this study indicate thermal degradation and it is caused by thermal decomposition, the stable processing region of 200 μm pitch should be EMR<6. Thus, the maximum UTS in the layering direction without thermal degradation would be 17–30 MPa.

Finally, this paper discusses processing in a layer pitch of 300 μm. Although building the specimen is difficult owing to the insufficient connectivity between the layers, smoke is already generated at an energy of EMR < 4.8, and thermal degradation is a concern. Therefore, the maximum UTS in the layering direction without thermal degradation was less than 8 MPa. If smoke generation or thermal degradation is disregarded, it may be possible to achieve a higher UTS by increasing the input energy, such as EMR > 7.6. At EMR < 7.6, it is suggested that the promotion of the connection of the layers is more dominant in improving the mechanical properties in the layer direction than the influence of thermal degradation. However, according to the rough simulation shown in Figure 8, the calculated temperature of the processing region exceeds 580 ℃, which is significantly higher than the thermal decomposition temperature of PA11 (approximately 350 ℃ reported by Ferry et al.[22]). In addition, although the block-shaped specimen could obtain a relatively high density, the density of the dog bone-shaped specimen with a small horizontal cross-section was smaller than that of the block-shaped specimen, as shown in Figure 9. The maximum value did not reach 90%, and there was a decreasing tendency for EMR > 6.9. Therefore, it is unlikely that higher energy inputs for 300 μm pitch will result in higher mechanical properties than in 100 or even 200 μm pitch. Moreover, it is undesirable and impractical not only because of the degradation of polymer materials but also because of the pollution of PBF-LB/P machines and optical systems such as windows and lenses.

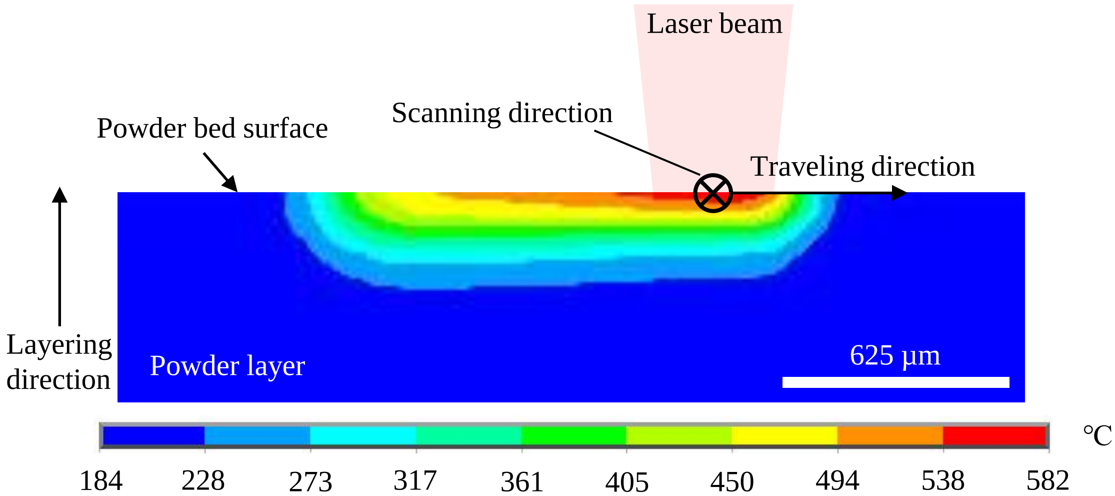

Figure 8 Temperature in processing region estimated by FEM analysis for 300 μm pitch with EMR 7.6. This approximate simulation was conducted using ANSYS, based on transient heat transfer analysis, employing the method previously reported by the authors[23]. The thermal conductivity of the powder and the thermal transfer between the powder bed and the nitrogen atmosphere of the chamber were set to 0.26 W/m·K and 50 W/m^2·K, respectively. It is assumed that the penetration depth of the powder bed with CO_2 laser and PA11 is 80 μm and the reflectance is 6% including specular and diffuse reflection, based on previous reports.

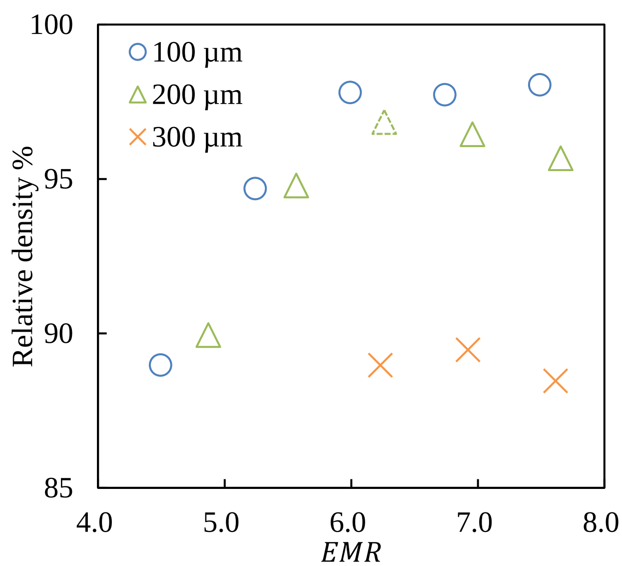

Figure 9 Relative density of dog bone-shaped specimens. For only 200 μm pitch of EMR 6.3 (the plot is shown as a dotted line), the density of the specimen was measured after the tensile test. This result is based on a single sample in each condition.

Conclusion

This study focuses on expanding the layer pitch to improve the processing speed of PBF-LB/P. The specimens were prepared under various conditions, and certain indices were implemented for each layer pitch for comparison. The mechanical properties, particularly tensile strength in the layering direction, which is affected by the layer pitch, were investigated. Simultaneously, smoke and spark generation were observed during the process to validate whether the process was performed in a stable region without thermal degradation. The following conclusions were drawn from this study. The achieved UTS, which avoided thermal degradation, was 46–50, 17–29, and <8 MPa for a layer pitch of 100, 200, and 300 μm, respectively. If smoke generation is permitted, the maximum UTS is 34 and 31 MPa for 200 and 300 μm pitch, respectively. Consequently, the decline in the mechanical properties that accompany layer pitch expansion is unavoidable in the current method, necessitating the fundamental development of the PBF-LB/P process.

Acknowledgment

This study was supported by the METI R&D Support Program for Growth-Oriented Technology SMEs (Grant number JPJ005698).

References

[1] Salmi, M., Akmal, J. S., Pei, E., Wolff, J., Jaribion, A., and Khajavi, S. H., 2020, "3D Printing in COVID-19: Productivity Estimation of the Most Promising Open Source Solutions in Emergency Situations," Appl. Sci., **10**(11), pp. 1–15.

[2] Liao, J., De Kleine, R., Kim, H. C., Luckey, G., Forsmark, J., Lee, E. C., and Cooper, D. R., 2023, "Assessing the Sustainability of Laser Powder Bed Fusion and Traditional Manufacturing Processes Using a Parametric Environmental Impact Model," Resour. Conserv. Recycl., **198**(November 2022), p. 107138.

[3] Sillani, F., MacDonald, E., Villela, J., Schmid, M., and Wegener, K., 2022, "In-Situ Monitoring of Powder Bed Fusion of Polymers Using Laser Profilometry," Addit. Manuf., **59**(PA), p. 103074.

[4] Gullane, A., Murray, J. W., Hyde, C. J., Sankare, S., Evirgen, A., and Clare, A. T., 2021, "On the Use of Multiple Layer Thicknesses within Laser Powder Bed Fusion and the Effect on Mechanical Properties," Mater. Des., **212**, p. 110256.

[5] Wegner, A., and Witt, G., 2012, "Correlation of Process Parameters and Part Properties in Laser Sintering Using Response Surface Modeling," Phys. Procedia, **39**, pp. 480–490.

[6] Pilipovic, A., Valentan, B., Brajlih, T., Haramina, T., Balic, J., Kodvanj, J., Sercer, M., and Drstvensek, I., 2010, "Influence of Laser Sintering Parameters on Mechanical Properties of Polymer Products," Ann. DAAAM Proc. Int. DAAAM Symp., pp. 285–286.

[7] Wegner, A., Harder, R., Witt, G., and Drummer, D., 2015, "Determination of Optimal Processing Conditions for the Production of Polyamide 11 Parts Using the Laser Sintering Process," Int. J. Recent Contrib. from Eng. Sci. IT, **3**(1), p. 5.

[8] Starr, T. L., Gornet, T. J., and Usher, J. S., 2011, "The Effect of Process Conditions on Mechanical Properties of Laser-Sintered Nylon," Rapid Prototyp. J., **17**(6), pp. 418–423.

[9] Zehir, B., Seyedzavvar, M., and Boğa, C., 2024, “Exploring Mixed-Mode Fracture Behavior and Mechanical Properties of Selective Laser Sintered Polyamide 12 Components,” Rapid Prototyp. J., **30**(3), pp. 529–546.

[10] Hofland, E. C., Baran, I., and Wismeijer, D. A., 2017, “Correlation of Process Parameters with Mechanical Properties of Laser Sintered PA12 Parts,” Adv. Mater. Sci. Eng., **2017**.

[11] Peyre, P., Rouchausse, Y., Defauchy, D., and Régnier, G., 2015, “Experimental and Numerical Analysis of the Selective Laser Sintering (SLS) of PA12 and PEKK Semi-Crystalline Polymers,” J. Mater. Process. Technol., **225**, pp. 326–336.

[12] Yamauchi, Y., Kigure, T., Isoda, K., and Niino, T., 2021, “Powder Bed Penetration Depth Control in Laser Sintering and Effect on Depth of Fusion,” Addit. Manuf., **46**(July), p. 102219.

[13] Yamauchi, Y., Kigure, T., and Niino, T., 2023, “Penetration Depth Optimization for Proper Interlayer Adhesion Using Near-Infrared Laser in a Low-Temperature Process of PBF-LB/P,” J. Manuf. Process., **98**(October 2022), pp. 126–137.

[14] Osmanlic, F., Wudy, K., Laumer, T., Schmidt, M., Drummer, D., and Körner, C., 2018, “Modeling of Laser Beam Absorption in a Polymer Powder Bed,” Polymers (Basel)., **10**(7), pp. 1–11.

[15] Budden, C. L., Lalwani, A. R., Meinert, K. Æ., Daugaard, A. E., and Pedersen, D. B., 2022, “Process Optimisation of PA11 in Fiber-Laser Powder-Bed Fusion through Loading of an Optical Absorber,” Proc. 33rd Annu. Int. Solid Free. Fabr. Symp., pp. 75–86.

[16] Yamauchi, Y., Kigure, T., and Niino, T., 2023, “Quantification of Supplied Laser Energy and Its Relationship with Powder Melting Process in PBF-LB/P Using near-Infrared Laser,” J. Manuf. Process., **99**(May), pp. 272–282.

[17] Vasquez, M., Haworth, B., and Hopkinson, N., 2012, “Methods for Quantifying the Stable Sintering Region in Laser Sintered Polyamide-12,” Polym. Eng. Sci., **53**(6), pp. 1230–1240.

[18] Alkema, “RILSAN® Fine Powders (Invent Grades)” [Online]. Available: https://hpp.arkema.com/en/product-families/rilsan-.

[19] Zarringhalam, H., Majewski, C., and Hopkinson, N., 2009, “Degree of Particle Melt in Nylon-12 Selective Laser-Sintered Parts,” Rapid Prototyp. J., **15**(2), pp. 126–132.

[20] Dadbakhsh, S., Verbelen, L., Vandeputte, T., Strobbe, D., Van Puyvelde, P., and Kruth, J. P., 2016, “Effect of Powder Size and Shape on the SLS Processability and Mechanical Properties of a TPU Elastomer,” Phys. Procedia, **83**, pp. 971–980.

[21] Ito, F., and Niino, T., 2016, “Implementation of Tophat Profile Laser into Low Temperature Process of Poly Phenylene Sulfide,” Solid Free. Fabr. 2016 Proc. 27th Annu. Int. Solid Free. Fabr. Symp. - An Addit. Manuf. Conf. SFF 2016, pp. 2194–2203.

[22] Ferry, L., Sonnier, R., Lopez-Cuesta, J. M., Petigny, S., and Bert, C., 2017, “Thermal Degradation and Flammability of Polyamide 11 Filled with Nanoboehmite,” J. Therm. Anal. Calorim., **129**(2), pp. 1029–1037.

[23] Kigure, T., Yamauchi, Y., and Niino, T., 2022, “Investigation into Effect of Beam Defocusing in Low Temperature Laser Sintering of PEEK,” Proc. 33rd Annu. Int. Solid Free. Fabr. Symp. – An Addit. Manuf. Conf., pp. 2271–2281.